Mapping nanoscale electric field hotspots of a plasmon-molecule system: a theoretical study

Junais Habeeb Mokkath*

Quantum Nanophotonics Simulations Lab, Department of Physics, Kuwait College of Science And Technology, Doha Area, 7th Ring Road, P.O. Box 27235, Kuwait.

E-mail: j.mokath@kcst.edu.kw

Abstract

The coherent interaction between localized surface plasmon resonance modes and excitons of a single or a collection of quantum emitters have fueled the development of novel applications in quantum optics and material science. In this work, using first-principles simulations, we analyse the modifications in absorption spectra and electric near-field enhancements in a structure consisting of an aluminum nanotriangle interacting with a varying number of pyridine molecules (placed at the nanotriangle tips) in close proximity. What's more, we find very interesting spatial variation in induced electron density and electric near-field enhancements with a remarkable dependence on the number of interacting pyridine molecules and the direction of light illumination. Our results may help to improve our understanding of the light-matter interaction at the sub-nanometer scale.

Introduction

Coupling excitons (bound electron-hole pairs) and plasmons (collective oscillations of conduction electrons in metals) in hybrid nanostructures have been utilized for a variety of applications including lasers,[1] control of chemical reactivity,[2] quantum information processing,[3] all optical logics,[4] light-matter strong coupling[5] and many other nanophotonic applications. Generally, a molecule couples weakly to a photon due to the large size mismatch. This mismatch can be substantially reduced by placing a molecule in an optical cavity.[6] In this context, a wide range of optical cavities as diverse as Fabry-Perot resonators to nanoscale plasmonic cavities has been proposed. When placed in plasmonic cavities, excitons can strongly mix with the cavity modes and form exciton-plasmon excitations.[7,8] More recently, it was shown that the plasmonic cavities greatly enhance the interaction between plasmons and excitons.[9] A widely used strategy to achieve intense plasmonic cavity ("hotspot regions") is to form anisotropic nanoparticles (NPs) with sharp tips.[10–13] Among the large variety of anisotropic NPs that have been created, nanotriangles render interesting features as far as the plasmonic hotspots are concerned. By shrinking the effective plasmon mode volume, the metal nanotriangle can localize an enormous amount of electromagnetic field at the tips.[14–16]

It is challenging to provide an in-depth understanding of plasmon-exciton excitations through experimental methods alone due to the difficulty in finding the actual contributions from different physico-chemical processes. In this context, complementary theoretical calculations and computer simulations can provide highly informative insights as they enable scrutinizing the relevant processes. It is the purpose of this paper to theoretically investigate the spatial modulations of induced charge density and electric near-field enhancement of a nanosystem consisting of a metal nanotriangle interacting with one to three pyridine molecules positioned at the nanotriangle tips. We chose nanotriangles made up of aluminum (Al).[17] It is an earth-abundant metal with high plasma frequency and emerged as a competitor to the coinage metals like Au and Ag for plasmonics applications. It has been reported that, depending on the size and shape, Al NPs support localized surface plasmon resonances

(LSPRs) that span the electromagnetic spectrum from the ultraviolet into the infrared.[18–27] Al is also compatible with complementary metal-oxide semiconductor manufacturing techniques.[28]

From a theoretical point of view, classical optics simulations are appropriate to design plasmonic devices with desired optical features. Nevertheless, recent quantum mechanical calculations reported that when one or more dimension(s) of a nano-object shrink to nanometer or sub-nanometer size range, quantum effects such as the electron confinement and the spill out of the electrons outside the nano-object surface start to become important.[29–33] In the case of nanotriangles, given a large surface-to-volume ratio, classical optics simulations that consider the surface as a sharp discontinuous potential cannot be reliable. This situation usually demands a fully quantum mechanical framework that takes into account the quantum nature of the electrons in their interaction with light. One of the efficient and computationally viable methods is the time dependent density functional theory (TD-DFT) technique. It is a standard simulation tool for modeling plasmonic response from a quantum-mechanical perspective. Moreover, TD-DFT technique allows the whole system (Al nanotriangle and pyridine molecules) to be treated on the same footing. What is observed in this investigation is that both the induced charge density and electric near-field enhancements display a remarkable sensitivity to the number of interacting pyridine molecules and the direction of light illumination. The rest of this paper is organized as follows. In the next section, we illustrate our model structures and the simulation methods employed. We show our results and discuss them in the next section, addressing the absorption spectra, electronic structure, induced charge density and electric near-field enhancements. The conclusions and outlook section closes the paper.

Systems and Model

The TD-DFT calculations in this work are performed using the open-source GPAW software package (version number 1.5.2)[34,35] in combination with atomic simulation environment (ASE)[36] and local density approximation (LDA)[37,38] exchange-correlation functional. The time-dependent wavefunctions, electron density, and potentials were evaluated on a uniform real-space grid with a spacing of 0.3 Å. Al nanotriangle is composed of 28 atoms with an approximate tip-to-tip distance of 1.70 nm, see Fig. 1. The investigated systems were placed into a cubic unit cell with the vacuum size of 10 Å along all principal directions. We employed TD-DFT technique (linear-response regime) in the frequency space[39–45] based on the Casida equation expressed in the Kohn-Sham electron-hole space.[46] The Casida approach directly enables a decomposition of the electronic excitations into the underlying Kohn-Sham electron-hole transitions, which readily yields quantum-mechanical understanding of the plasmonic response. In the same context, the number of dipole-allowed transitions (roots) should be large enough to span the desired range in the absorption spectrum. We found that 1284 roots are needed to plot the absorption spectrum of Al nanotriangle in the energy range of 0 of 10 eV. As expected, in the case of Al nanotriangle attached to one/two/three pyridine molecules, we found 2064/2821/3219 roots are needed to plot the absorption spectra in the energy range between 0 of 10 eV. All absorption spectra are broadened by a Gaussian smearing of width $\sigma = 0.10$ eV. The induced charge density is obtained directly from the linear response of the electron density: $\delta\rho(r,\omega) = -\sum_{\sigma}\sum_{ij}\psi_{i\sigma}(\mathbf{r})\psi^{*}_{j\sigma}(\mathbf{r})\delta P_{ij\sigma}(\omega)$, where $\psi_{i\sigma}(\mathbf{r})$ and $\psi^{*}_{j\sigma}$ are the unperturbed and perturbed Kohn-Sham states, respectively, and $P_{ij\sigma}(\omega)$ is the density matrix. Using the calculated induced charge density, we computed the electric near-field enhancement (defined as a ratio between the total electric field and the perturbing electric field) using $E_{fe}(r,\omega) = \dfrac{|E_{ext}(\mathbf{r},\omega) + \delta E(\mathbf{r},\omega)|}{|E_{ext}(\mathbf{r},\omega)|}$, where in the dipole approximation the perturbing field is spatially constant, i.e. $|E_{ext}(\mathbf{r},\omega)| = |E(\mathbf{r},\omega)|$.[47,48] We remark that before the TD-DFT calculations, we performed DFT ground state calculations with a set of

unoccupied states. We have incorporated 200 unoccupied states to the DFT ground state calculation and all these states have been employed to construct the Casida matrix. Only the 3 valance electrons of Al atoms were explicitly included in the calculations and other electrons were treated as a frozen core. Consequently, the number of valence electrons in our Al nanotriangle is 84. We remark that the free-electron-like electronic structure of Al further simplified the TD-DFT calculations.

Results and Discussion

It is important to begin this work with understanding the absorption spectrum (in the energy range of 0 to 10 eV) of the constituent systems: the individual Al nanotriangle and pyridine molecule, see Fig. 1. Note that Al nanotriangle possesses an asymmetric shape. Therefore, we plot the absorption spectrum for the perturbing electric field aligned along the system's x- and z-directions (see Fig. 1) represented by Al(x) and Al(z), respectively. We would like to stress that although Al(x) and Al(z) absorption spectra look more or less similar, their absorption peaks exhibit remarkably distinct features as far as the induced charge density and electric near-field enhancements are concerned (see the next section for more details).

Next, we analyse the similarities and differences in the Al(x) and Al(z) absorption spectra. In the case of Al(x), we find a pronounced (dominant) peak centered at around 3.45 eV (with a total absorption value of 142 eV^{-1}) and a low-intensity peak centered at around 5.87 eV (with a total absorption value of 35 eV^{-1}). In the case of Al(z), we find a pronounced (dominant) peak centered at around 3.45 eV (with a total absorption value of 150 eV^{-1}) and a low-intensity peak centered at around 5.82 eV (with a total absorption value of 33 eV^{-1}). To gain more details regarding the nature of the absorption peaks, we analyse the total number of contributing electron$-$hole transitions that make up each absorption peak. We found that the dominant absorption peak centered at around 3.45 eV is composed of many electron$-$hole transitions. Specifically, 3.45 eV and 5.87 eV peaks of Al(x) are composed

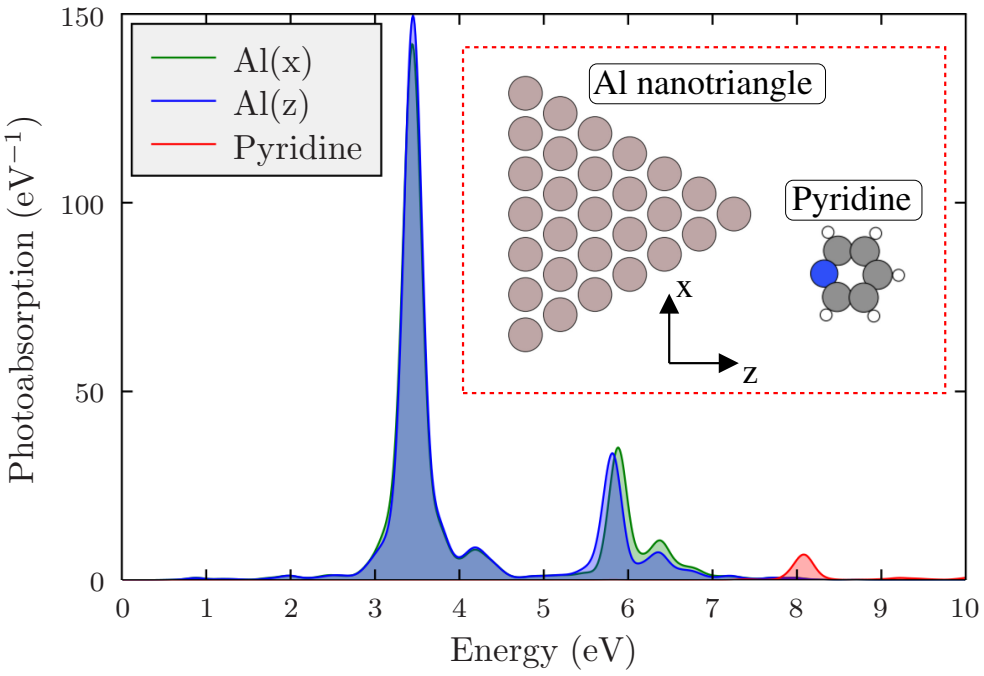

Figure 1: TD-DFT calculated photoabsorption spectra of the individual Al nanotriangle and pyridine molecule in the energy range between 0 to 10 eV. Al(x) and Al(z) represents the photoabsorption spectra along the x- and z-directions, respectively. In the inset, the chemical structure of individual Al nanotriangle (tip-to-tip distance of 1.70 nm) and pyridine molecule under study.

of 32 and 4 electron−hole transitions, respectively. Whereas 3.45 eV and 5.82 eV peaks of Al(z) are characterized by 35 and 4 electron−hole transitions, respectively. It is worth to recall that quantum mechanically, the contribution from a large number of electron−hole transitions to an absorption peak indicates a strong collectivity in the optical excitation. On the other hand, in the case of the pyridine molecule, we find absorption peaks centered at around 8.10 eV and 9.21 eV with a total absorption value of 6.75 eV^{-1} and 0.60 eV^{-1}, respectively.

Next, we analyse the induced charge density (δn) and electric near-field enhancement (E_{fe}) corresponding to the Al(x) and Al(z) main absorption peaks. This analysis will provide useful insight into the plasmonic nature of the absorption peaks. It is worthwhile to emphasize that one of the highly desired characteristics of an optical nanoantenna is its ability to localize E_{fe} to ultra-small nanoscale volumes. First, we analyse δn and E_{fe} cor-

responding to the Al(x) absorption peaks centered at around 3.45 eV and 5.87 eV, see the left panel in Fig. 2. Evidently, the nodal structure of δn is highly distinct for the 3.45 eV and 5.87 eV peaks (see the top row in the left panel of Fig. 2). While 3.45 eV peak displays a single-node dipole-like electron density distribution, 5.87 eV peak shows a multi-nodal quadruple-like electron density distribution. Also, it is interesting to see that the maximal absolute value of δn (i. e.; $|\delta n|$) of the first peak is almost double in comparison to the second peak. Now let us analyse E_{fe} corresponding to the Al(x) peaks, see the bottom row in the left panel of Fig. 2. As states before, E_{fe} plot allows us to visualize the plasmonic hotspot regions. In the case of 3.45 eV peak, the hotspot regions are located mainly at the two tips with a maximal absolute value of the electric field "$|E_{fe}|$" of 144. Note that both the E_{fe} and $|E_{fe}|$ are substantially different in the case of 5.87 eV peak. One finds that E_{fe} is distributed more or less entirely over the nanotriangle with a $|E_{fe}|$ value of 92. Now let us analyse the δn and E_{fe} corresponding to the Al(z) absorption peaks centered at around 3.45 eV and 5.82 eV, see the right panel in Fig. 2. One can easily identify the differences in δn, $|\delta n|$, E_{fe} and $|E_{fe}|$ in comparison to the Al(x) results. For example, in the case of 3.45 eV peak, one remarkable feature of the E_{fe} is that it is almost fully confined to the tip located at the right corner with a $|E_{fe}|$ value of 220. This, in turn, implies that Al(z) absorption peaks would be more interacting with pyridine molecules than Al(x) absorption peaks (most likely due to enhanced coupling strengths). To summarize this analysis, we remark that Al nanotriangle renders plasmon-like induced charge density and electric near-field distribution constituting unambiguous shreds of evidence of a plasmonic nanoantenna. Most importantly, we can clearly identify sub-nanometric 'hot-spots' characterized by strongly localized fields at the nanotriangle tips.

After discussing the δn and E_{fe} features of the individual Al nanotriangle, now we attempt a similar analysis in the case of pyridine molecule, see Fig. 3. Apparently, one finds that $|\delta n|$ and $|E_{fe}|$ values are much larger for the absorption peak centered at around 8.10 eV in comparison to the 9.21 eV peak. More specifically, $|\delta n|$ and $|E_{fe}|$ value for the 8.10 eV

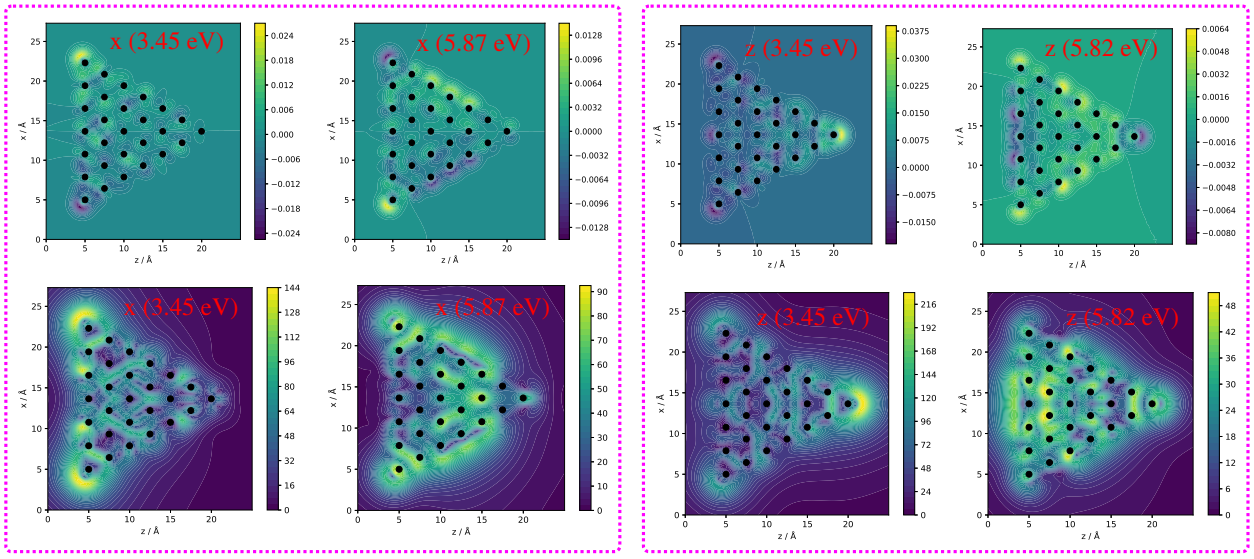

Figure 2: Illustrating the δn and E_{fe} of the Al nanotriangle. In the left panel, we show δn and E_{fe} corresponding to the Al(x) peaks centered at around 3.45 eV and 5.87 eV. In the right panel, we show δn and E_{fe} corresponding to the Al(z) peaks centered at around 3.45 eV and 5.82 eV.

peak is 0.033 and 134, respectively. However, in the case of 9.21 eV peak, $|\delta n|$ and $|E_{fe}|$ value is 0.003 and 27, respectively. This result suggests that when attached to the Al nanotriangle tip, the absorption peak centered at around 8.10 eV will be more interacting with the Al nanotriangle absorption peaks.

After analysing the absorption features, δn and E_{fe} features of the individual Al nanotriangle and pyridine molecule, we next carry out a similar analysis in the case of the hybrid systems. First, we start with the analysis of the absorption features and electronic structure via orbital-projected DOS of the Al nanotriangle interacting with a pyridine molecule (Al+P1), see the top row of Fig. 4. It is highly evident that the absorption spectrum of Al+P1 system is strongly direction dependent as a result of the symmetry breaking in the system induced by the attachment of the pyridine molecule. We observe sharper absorption peaks along the x-direction while the absorption peaks along the z-direction are broadened. This is not surprising considering the fact that the interaction of the pyridine molecule with the Al nanotriangle will be increased along the z-direction. It is evident that, along the x-direction, there emerges four peaks centered at around 3.43 eV, 4.24 eV, 6.05 eV, and 8.32

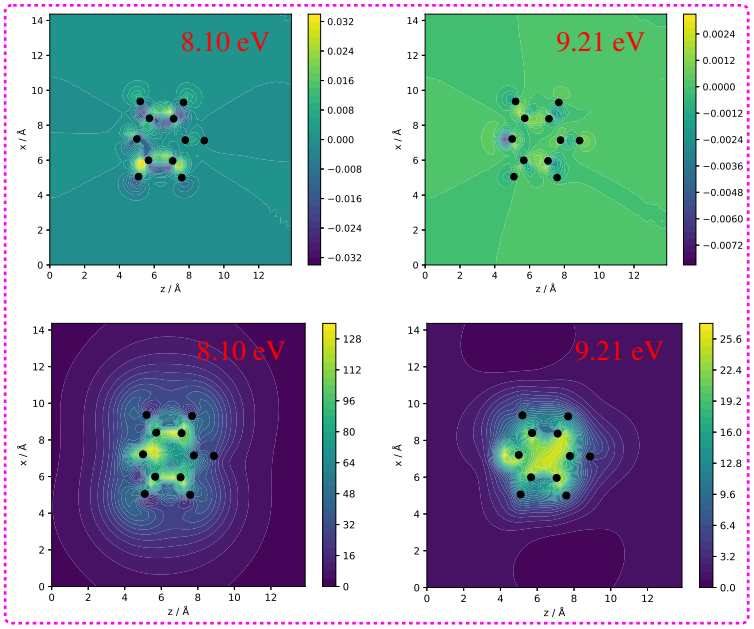

Figure 3: Illustrating the δn and E_{fe} corresponding to the 8.10 eV and 9.21 eV absorption peaks of the pyridine molecule.

eV, respectively, with a total absorption value of 127 eV^{-1}, 9 eV^{-1}, 26 eV^{-1} and 9 eV^{-1}, respectively. Along the z-direction, there emerges four peaks centered at around 3.46 eV, 4.26 eV, 5.93 eV, and 8.32 eV, respectively, with a total absorption value of 100 eV^{-1}, 10 eV^{-1}, 23 eV^{-1} and 3 eV^{-1}, respectively. On the other hand, the orbital-projected DOS analysis shows that the states around the Fermi level are mainly contributed by the Al s and p states. One also finds the presence of C p states below (4.2 eV) and above (0.70 eV) the Fermi level with a negligibly minor presence of C s states. In addition, one also observes unoccupied N p states above the Fermi level. These results suggest that the optical excitations between the Al nanotriangle and the pyridine molecule will occur mainly due to the electronic transitions between Al s/p states and C p / N p states. After analysing the absorption features and orbital-projected DOS corresponding to the Al+P1 system, it is informative to analyse the δn and E_{fe} features along the x- and z-directions. First, we consider the x-direction, see the top panel in Fig. 5. Note that δn is shown on the top and the corresponding E_{fe} plots are shown at the bottom. As seen in Fig. 4, Al+P1 absorption features along the x-direction is characterized by four peaks centered at around 3.43 eV, 4.24 eV, 6.05 eV, and 8.32 eV. The

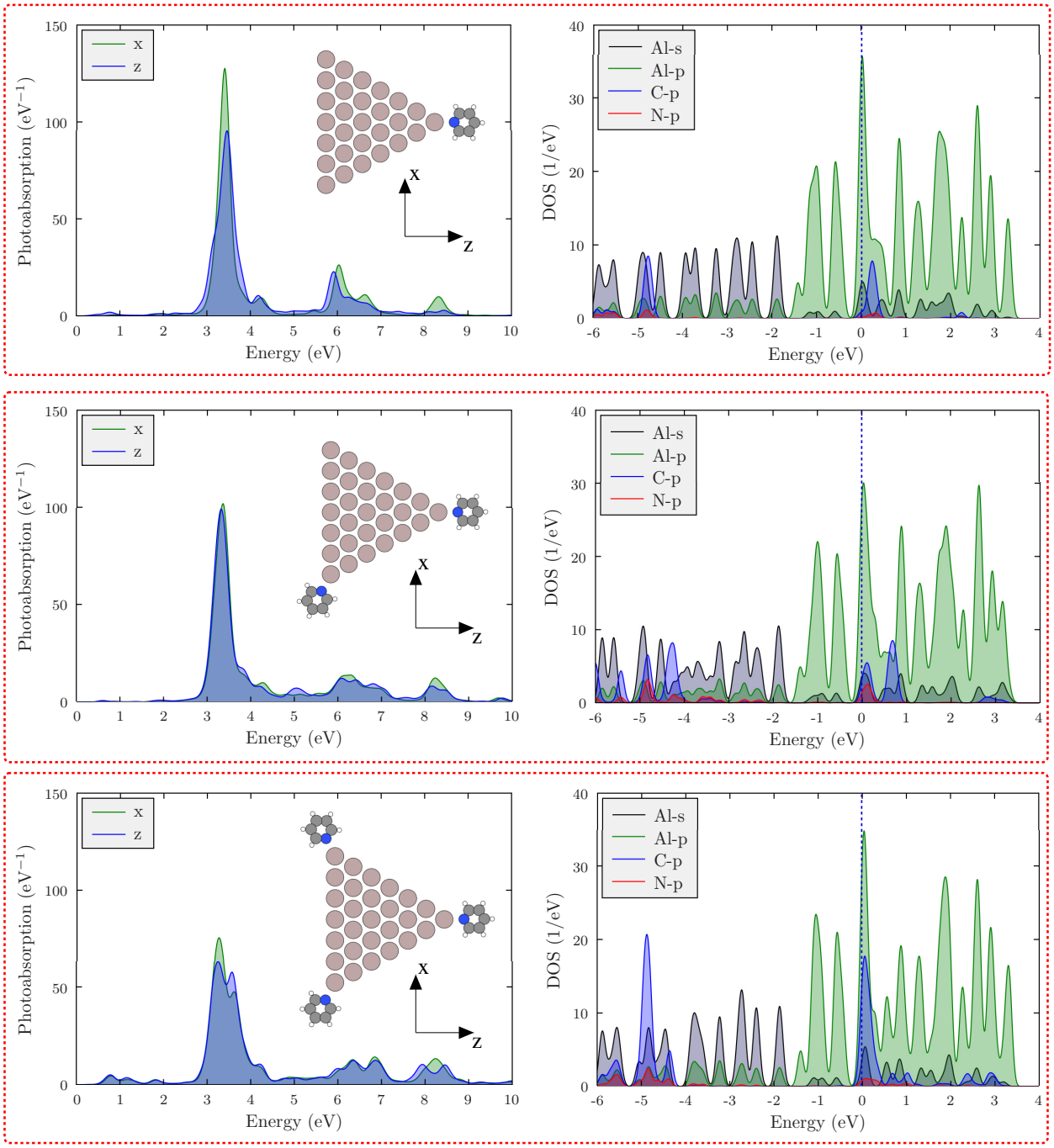

Figure 4: TD-DFT calculated photoabsorption spectra and orbital-projected density of states (DOS) of the hybrid systems. In the top: Al+P1 system consisting of an Al nanotriangle interacting with a pyridine molecule. In the middle: Al+P2 system consisting of an Al nanotriangle interacting with two pyridine molecules. In the bottom: Al+P3 system consisting of an Al nanotriangle interacting with three pyridine molecules. The dashed blue-lines in the orbital-projected DOS indicates the Fermi level.

top panel in Fig. 5 shows that, for the first three peaks, both the δn and E_{fe} is almost fully confined to the Al nanotriangle itself. However, the scenario is different in the case of 8.32 eV peak. In particular, both the δn and E_{fe} is distributed over the pyridine molecule. We further inspect δn and E_{fe} modulations along the z-direction, see the bottom panel in Fig. 5. In the case of the first three peaks centered at around 3.46 eV, 4.26 eV, 5.93 eV, one finds that both δn and E_{fe} are distributed over the Al nanotriangle and the regions connecting the Al nanotriangle and pyridine molecule. However, in the case of 8.32 eV peak, as expected, both δn and E_{fe} are mainly confined to the pyridine molecule only. These findings indicate that the optical interaction between the Al nanotriangle and pyridine molecule is strongly sensitive to the direction of the light illumination.

Next, we analyse the absorption profile, electronic structure, δn and E_{fe} features of the Al+P2 system. The middle panel in Fig. 4 shows clear differences in the absorption features along the x- and z-directions but not as dramatic as in the case of Al+P1 system. A notable difference in the absorption features (both in the absorption intensity and energetic position of the absorption peaks) emerges in the case of the dominant peak. More specifically, the dominant peak along the x-direction is centered at around 3.37 eV with a total absorption value of 101 eV^{-1}. Whereas, the dominant absorption peak along the z-direction is centered at around 3.34 eV with a total absorption value of 98 eV^{-1}. The reduction in the total absorption value and red-shift of the absorption peak along the z-direction can be attributed to the increased optical interaction between the Al nanotriangle and pyridine molecules. Also, we observe minor differences in the other absorption peaks as well. Analysing the orbital-projected DOS of the Al+P2 system shows that the unoccupied C p and N p states are now more close to the Fermi level (favorable for the electronic transitions between Al s/p states and C p / N p states). After having analysed the absorption features and electronic structure of the Al+P2 system, it is important to analyse δn and E_{fe} features along the x- and z-directions. First, we start with x-direction, see the top panel in Fig. 6. Note that, we analyse δn and E_{fe} features corresponding to the peaks centered at around 3.37 eV, 6.22

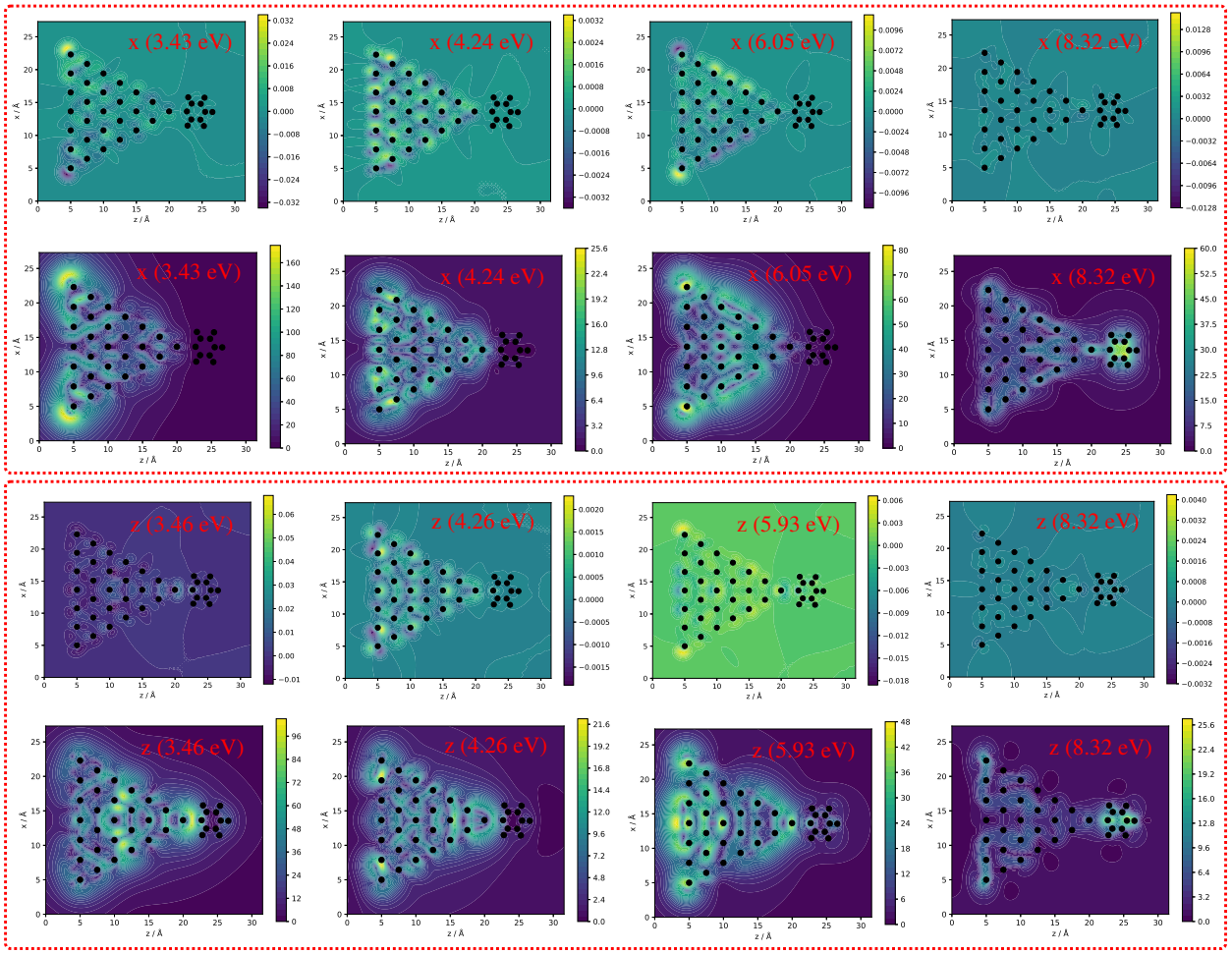

Figure 5: Illustrating the δn and E_{fe} corresponding the absorption peaks of Al+P1 system. In the top panel, we show δn and E_{fe} along the x-direction for the peaks centered at around 3.43 eV, 4.24 eV, 6.05 eV, and 8.32 eV. In the bottom panel, we show δn and E_{fe} along the z-direction for the peaks centered at around 3.46 eV, 4.26 eV, 5.93 eV, and 8.32 eV.

eV, and 8.24 eV. First, as a key observation, both $|\delta n|$ and $|E_{fe}|$ values of the dominant absorption peak is significantly reduced in comparison to the dominant peak corresponding to the Al+P1 system. Also one finds that δn and E_{fe} corresponding to the first two peaks are distributed over the Al nanotriangle and the region connecting the Al nanotriangle and pyridine molecules. Nevertheless, 8.24 eV peak is solely contributed by the two pyridine molecules. The situation is different in the case of z-direction, see the bottom panel in Fig. 6. As in the case of Al+P1 system, the optical interaction between the Al nanotriangle and pyridine molecules is expected to be stronger along the z-direction than along the x-direction.

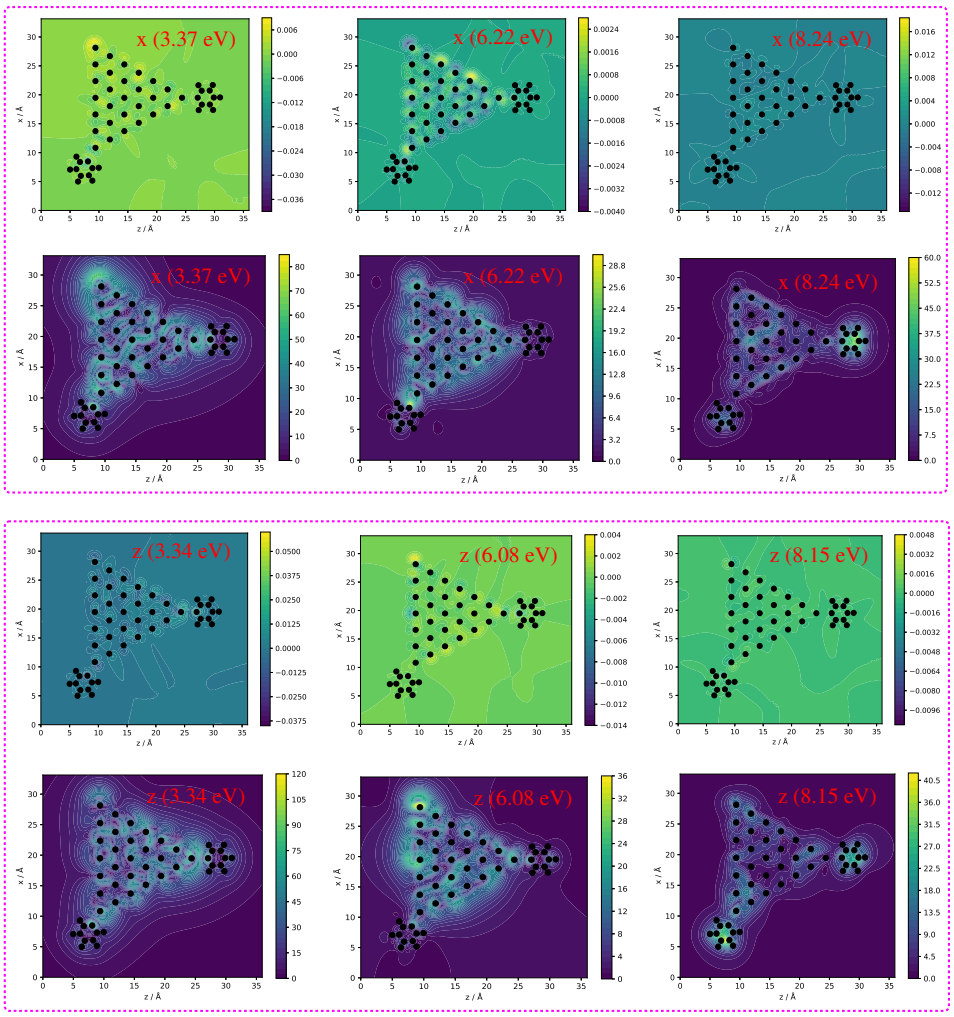

Figure 6: Illustrating the δn and E_{fe} corresponding the absorption peaks of Al+P2 system. In the top panel, we show δn and E_{fe} along the x-direction for the peaks centered at around 3.37 eV, 6.22 eV, and 8.24 eV. In the bottom panel, we show δn and E_{fe} along the z-direction for the peaks centered at around 3.34 eV, 6.08 eV, and 8.15 eV.

In particular, for the peaks centered at around 3.34 eV and 6.08 eV, one finds sizable δn and E_{fe} enhancements in the regions connecting the Al nanotriangle and pyridine molecules. Nevertheless, in the case of 8.15 eV peak, as expected, both δn and E_{fe} are confined to the pyridine molecules only.

In what follows, we proceed to analyse the absorption features, electronic structure, δn and E_{fe} for the Al+P3 system. First, we analyse the absorption features and electronic structure, see the bottom part in Fig. 4. Let us first analyse the absorption peaks along the x-direction: 3.26 eV (with a total absorption value of 76 eV^{-1}), 6.36 eV (with a total

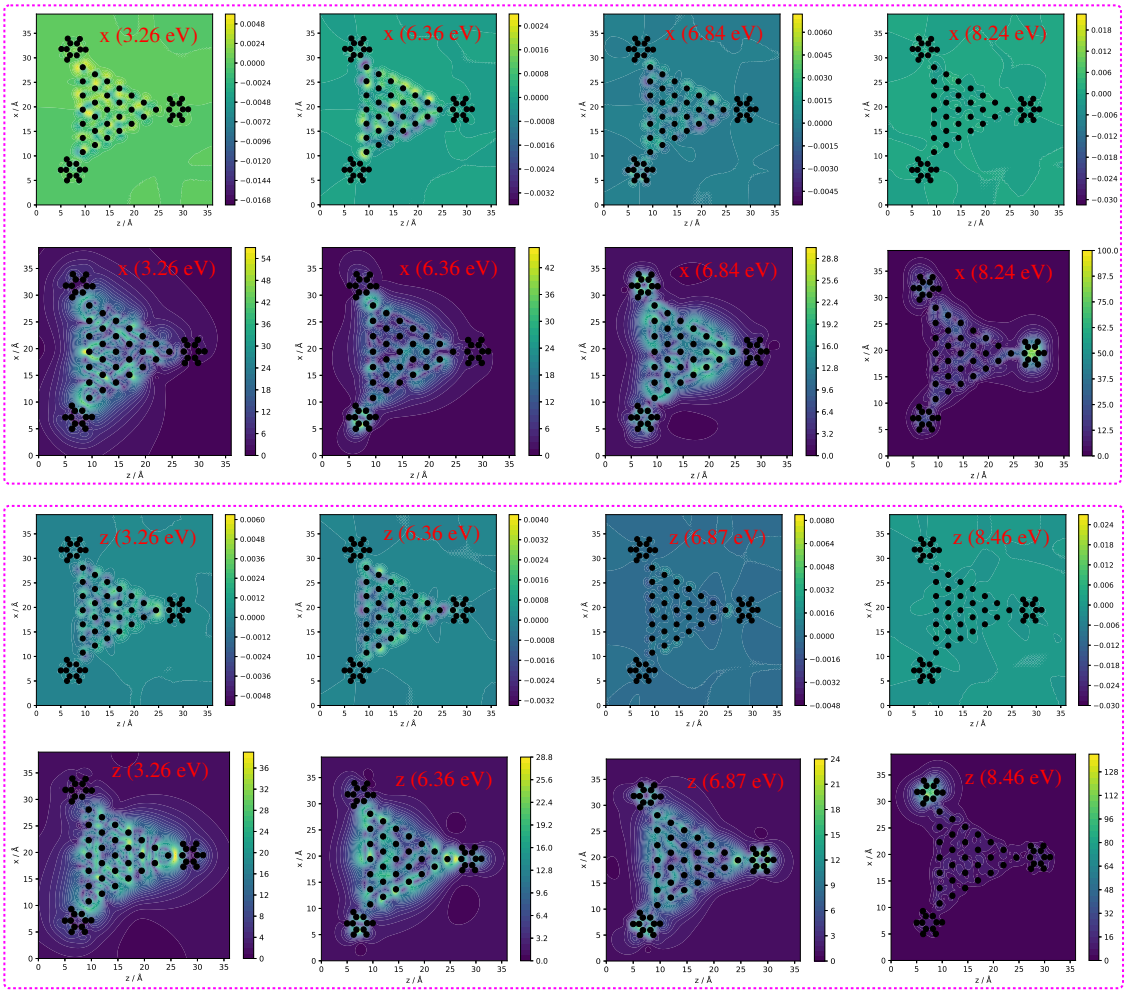

Figure 7: Illustrating the δn and E_{fe} corresponding to the Al+P3 system. In the top panel, we show δn and E_{fe} along the x-direction for the peaks centered at around 3.26 eV, 6.36 eV, 6.84 eV, and 8.24 eV. In the bottom panel, we show δn and E_{fe} along the z-direction for the peaks centered at around 3.26 eV, 6.36 eV, 6.87 eV, and 8.46 eV.

absorption value of 13 eV^{-1}), 6.84 eV (with a total absorption value of 14 eV^{-1}) and 8.24 eV (with a total absorption value of 13 eV^{-1}). Let us now analyse the absorption peaks along the z-direction: 3.26 eV (with a total absorption value of 63 eV^{-1}), 6.36 eV (with a total absorption value of 12 eV^{-1}), 6.87 eV (with a total absorption value of 12 eV^{-1}) and 8.46 eV (with a total absorption value of 9 eV^{-1}). The orbital-projected DOS shows that the unoccupied C p states are significantly enhanced and the contribution of N p states near the Fermi level is more distributed. After having analysed the absorption features and the electronic structure of the Al+P3 system, a comprehensive visual understanding of δn and

E_{fe} can be obtained by analysing the features along the x- and z-directions. First, we start with the x-direction for the peaks centered at around 3.26 eV, 6.36 eV, 6.84 eV and 8.24 eV, see the top panel in Fig. 7. Our observation shows that δn and E_{fe} are distributed mostly on the Al nanotriangle and the regions connecting the nanotriangle and pyridine molecules for the first three absorption peaks. Nevertheless, the peaks centered at around 8.24 eV is fully contributed by the pyridine molecules. We now turn to the z-direction, see the bottom panel in Fig. 7. For the first three peaks, one finds sizable δn and E_{fe} values in the Al nanotriangle and regions connecting the Al nanotriangle and pyridine molecules. However, in the case of 8.46 eV peak, both the δn and E_{fe} are confined to one of the pyridine molecules only. To conclude this part, we remark that in realistic practical situations where the small organic molecules attached to the nanotriangle tips, there might be extra effects such as the thermal diffusion of the Al atoms at the tips. Thus, a more sophisticated theoretical treatment (for example, molecular dynamics plus TD-DFT) of the tip-molecule interface is required. Besides, if one wishes to explore the present hybrid systems experimentally, low-temperature experiments are needed to stabilize the system morphology.

Conclusions and outlook

In-depth understanding of the interaction between a quantum emitter and highly confined plasmonic cavity is vital for designing novel optical devices. Here, using the time-dependent density functional theory calculations, we have systematically analysed the spatial distributions of the induced charge density and electric near-field enhancements of a nanosystem consisting of an Al nanotriangle interacting with a varying number of pyridine molecules positioned at the tips. One of the key findings is electric near-field enhancements can be efficiently tuned by varying the number of interacting pyridine molecules and the direction of light illumination. To the best of our understanding, this is the first study quantum mechanically demonstrating the optical coupling between Al nanotriangle and pyridine molecules. In

a broader perspective, our quantum calculations provide opportunities to create the electric field hotspot regions at the nanoscale useful for designing ultra-small plasmonic devices and helps to improve our understanding of plasmon-molecule interactions at the sub-nanometer length scale.

Acknowledgement

The research reported in this publication was supported by funding from Kuwait College of Science And Technology (KCST).

References

(1) Schneider, C. et al. An electrically pumped polariton laser. *Nature* **2013**, *497*, 348–352.

(2) Munkhbat, B.; Wersäll, M.; Baranov, D. G.; Antosiewicz, T. J.; Shegai, T. Suppression of photo-oxidation of organic chromophores by strong coupling to plasmonic nanoantennas. *Science Advances* **2018**, *4*.

(3) Dzsotjan, D.; Sørensen, A. S.; Fleischhauer, M. Quantum emitters coupled to surface plasmons of a nanowire: A Green's function approach. *Phys. Rev. B* **2010**, *82*, 075427.

(4) Liew, T. C. H.; Kavokin, A. V.; Shelykh, I. A. Optical Circuits Based on Polariton Neurons in Semiconductor Microcavities. *Phys. Rev. Lett.* **2008**, *101*, 016402.

(5) Li, R.-Q.; Hernángomez-Pérez, D.; García-Vidal, F. J.; Fernández-Domínguez, A. I. Transformation Optics Approach to Plasmon-Exciton Strong Coupling in Nanocavities. *Phys. Rev. Lett.* **2016**, *117*, 107401.

(6) Neuman, T.; Esteban, R.; Casanova, D.; García-Vidal, F. J.; Aizpurua, J. Coupling of Molecular Emitters and Plasmonic Cavities beyond the Point-Dipole Approximation. *Nano Letters* **2018**, *18*, 2358–2364, PMID: 29522686.

(7) Litz, J. P.; Brewster, R. P.; Lee, A. B.; Masiello, D. J. Molecular–Electronic Structure in a Plasmonic Environment: Elucidating the Quantum Image Interaction. *The Journal of Physical Chemistry C* **2013**, *117*, 12249–12257.

(8) Nascimento, D. R.; DePrince, A. E. Modeling molecule-plasmon interactions using quantized radiation fields within time-dependent electronic structure theory. *The Journal of Chemical Physics* **2015**, *143*, 214104.

(9) Rossi, T. P.; Shegai, T.; Erhart, P.; Antosiewicz, T. J. Strong plasmon-molecule coupling at the nanoscale revealed by first-principles modeling. *Nature Communications* **2019**, *10*, 3336.

(10) Zhang, Q.; Large, N.; Wang, H. Gold Nanoparticles with Tipped Surface Structures as Substrates for Single-Particle Surface-Enhanced Raman Spectroscopy: Concave Nanocubes, Nanotrisoctahedra, and Nanostars. *ACS Applied Materials & Interfaces* **2014**, *6*, 17255–17267, PMID: 25222940.

(11) Barbosa, S.; Agrawal, A.; Rodríguez-Lorenzo, L.; Pastoriza-Santos, I.; Alvarez-Puebla, R. A.; Kornowski, A.; Weller, H.; Liz-Marzán, L. M. Tuning Size and Sensing Properties in Colloidal Gold Nanostars. *Langmuir* **2010**, *26*, 14943–14950, PMID: 20804155.

(12) Khoury, C. G.; Vo-Dinh, T. Gold Nanostars For Surface-Enhanced Raman Scattering: Synthesis, Characterization and Optimization. *The Journal of Physical Chemistry C* **2008**, *112*, 18849–18859.

(13) Sanchez-Gaytan, B. L.; Swanglap, P.; Lamkin, T. J.; Hickey, R. J.; Fakhraai, Z.; Link, S.; Park, S.-J. Spiky Gold Nanoshells: Synthesis and Enhanced Scattering Properties. *The Journal of Physical Chemistry C* **2012**, *116*, 10318–10324.

(14) Keast, V. J.; Walhout, C. J.; Pedersen, T.; Shahcheraghi, N.; Cortie, M. B.; Mitchell, D.

R. G. Higher Order Plasmonic Modes Excited in Ag Triangular Nanoplates by an Electron Beam. *Plasmonics* **2016**, *11*, 1081–1086.

(15) Kumar, A.; Fung, K.-H.; Mabon, J. C.; Chow, E.; Fang, N. X. Excitation and imaging of resonant optical modes of Au triangular nanoantennas using cathodoluminescence spectroscopy. *Journal of Vacuum Science & Technology B* **2010**, *28*, C6C21–C6C25.

(16) Sherry, L. J.; Jin, R.; Mirkin, C. A.; Schatz, G. C.; Van Duyne, R. P. Localized Surface Plasmon Resonance Spectroscopy of Single Silver Triangular Nanoprisms. *Nano Letters* **2006**, *6*, 2060–2065, PMID: 16968025.

(17) Campos, A.; Arbouet, A.; Martin, J.; Gérard, D.; Proust, J.; Plain, J.; Kociak, M. Plasmonic Breathing and Edge Modes in Aluminum Nanotriangles. *ACS Photonics* **2017**, *4*, 1257–1263.

(18) Chan, G. H.; Zhao, J.; Schatz, G. C.; Van Duyne, R. P. Localized Surface Plasmon Resonance Spectroscopy of Triangular Aluminum Nanoparticles. *The Journal of Physical Chemistry C* **2008**, *112*, 13958–13963.

(19) Knight, M. W.; King, N. S.; Liu, L.; Everitt, H. O.; Nordlander, P.; Halas, N. J. Aluminum for Plasmonics. *ACS Nano* **2014**, *8*, 834–840, PMID: 24274662.

(20) Gérard, D.; Gray, S. K. Aluminium plasmonics. *Journal of Physics D: Applied Physics* **2014**, *48*, 184001.

(21) McClain, M. J.; Schlather, A. E.; Ringe, E.; King, N. S.; Liu, L.; Manjavacas, A.; Knight, M. W.; Kumar, I.; Whitmire, K. H.; Everitt, H. O.; Nordlander, P.; Halas, N. J. Aluminum Nanocrystals. *Nano Letters* **2015**, *15*, 2751–2755, PMID: 25790095.

(22) Clark, B. D.; Jacobson, C. R.; Lou, M.; Yang, J.; Zhou, L.; Gottheim, S.; DeSantis, C. J.; Nordlander, P.; Halas, N. J. Aluminum Nanorods. *Nano Letters* **2018**, *18*, 1234–1240, PMID: 29272131.

(23) Clark, B. D.; Jacobson, C. R.; Lou, M.; Renard, D.; Wu, G.; Bursi, L.; Ali, A. S.; Swearer, D. F.; Tsai, A.-L.; Nordlander, P.; Halas, N. J. Aluminum Nanocubes Have Sharp Corners. *ACS Nano* **2019**, *13*, 9682–9691, PMID: 31397561.

(24) Knight, M. W.; Liu, L.; Wang, Y.; Brown, L.; Mukherjee, S.; King, N. S.; Everitt, H. O.; Nordlander, P.; Halas, N. J. Aluminum Plasmonic Nanoantennas. *Nano Letters* **2012**, *12*, 6000–6004, PMID: 23072330.

(25) Tian, S.; Neumann, O.; McClain, M. J.; Yang, X.; Zhou, L.; Zhang, C.; Nordlander, P.; Halas, N. J. Aluminum Nanocrystals: A Sustainable Substrate for Quantitative SERS-Based DNA Detection. *Nano Letters* **2017**, *17*, 5071–5077, PMID: 28664736.

(26) Su, M.-N.; Dongare, P. D.; Chakraborty, D.; Zhang, Y.; Yi, C.; Wen, F.; Chang, W.-S.; Nordlander, P.; Sader, J. E.; Halas, N. J.; Link, S. Optomechanics of Single Aluminum Nanodisks. *Nano Letters* **2017**, *17*, 2575–2583, PMID: 28301725.

(27) Su, M.-N.; Ciccarino, C. J.; Kumar, S.; Dongare, P. D.; Hosseini Jebeli, S. A.; Renard, D.; Zhang, Y.; Ostovar, B.; Chang, W.-S.; Nordlander, P.; Halas, N. J.; Sundararaman, R.; Narang, P.; Link, S. Ultrafast Electron Dynamics in Single Aluminum Nanostructures. *Nano Letters* **2019**, *19*, 3091–3097, PMID: 30935208.

(28) Dabos, G.; Manolis, A.; Tsiokos, D.; Ketzaki, D.; Chatzianagnostou, E.; Markey, L.; Rusakov, D.; Weeber, J.-C.; Dereux, A.; Giesecke, A.-L.; Porschatis, C.; Wahlbrink, T.; Chmielak, B.; Pleros, N. Aluminum plasmonic waveguides co-integrated with Si3N4 photonics using CMOS processes. *Scientific Reports* **2018**, *8*, 13380.

(29) Halperin, W. P. Quantum size effects in metal particles. *Rev. Mod. Phys.* **1986**, *58*, 533–606.

(30) Townsend, E.; Bryant, G. W. Plasmonic Properties of Metallic Nanoparticles: The Effects of Size Quantization. *Nano Letters* **2012**, *12*, 429–434, PMID: 22181554.

(31) Zhang, P.; Feist, J.; Rubio, A.; García-González, P.; García-Vidal, F. J. Ab initio nanoplasmonics: The impact of atomic structure. *Phys. Rev. B* **2014**, *90*, 161407.

(32) García de Abajo, F. J. Nonlocal Effects in the Plasmons of Strongly Interacting Nanoparticles, Dimers, and Waveguides. *The Journal of Physical Chemistry C* **2008**, *112*, 17983–17987.

(33) David, C.; García de Abajo, F. J. Spatial Nonlocality in the Optical Response of Metal Nanoparticles. *The Journal of Physical Chemistry C* **2011**, *115*, 19470–19475.

(34) Mortensen, J. J.; Hansen, L. B.; Jacobsen, K. W. Real-space grid implementation of the projector augmented wave method. *Phys. Rev. B* **2005**, *71*, 035109.

(35) Walter, M.; Häkkinen, H.; Lehtovaara, L.; Puska, M.; Enkovaara, J.; Rostgaard, C.; Mortensen, J. J. Time-dependent density-functional theory in the projector augmented-wave method. *The Journal of Chemical Physics* **2008**, *128*, 244101.

(36) Larsen, A. H. et al. The atomic simulation environment—a Python library for working with atoms. *Journal of Physics: Condensed Matter* **2017**, *29*, 273002.

(37) Kohn, W.; Sham, L. J. Self-Consistent Equations Including Exchange and Correlation Effects. *Phys. Rev.* **1965**, *140*, A1133–A1138.

(38) Perdew, J. P.; Zunger, A. Self-interaction correction to density-functional approximations for many-electron systems. *Phys. Rev. B* **1981**, *23*, 5048–5079.

(39) Hsu, C.-P.; Hirata, S.; Head-Gordon, M. Excitation Energies from Time-Dependent Density Functional Theory for Linear Polyene Oligomers: Butadiene to Decapentaene. *The Journal of Physical Chemistry A* **2001**, *105*, 451–458.

(40) Silverstein, D. W.; Govind, N.; van Dam, H. J. J.; Jensen, L. Simulating One-Photon Absorption and Resonance Raman Scattering Spectra Using Analytical Excited

State Energy Gradients within Time-Dependent Density Functional Theory. *Journal of Chemical Theory and Computation* **2013**, *9*, 5490–5503, PMID: 26592284.

(41) Neugebauer, J. Couplings between electronic transitions in a subsystem formulation of time-dependent density functional theory. *The Journal of Chemical Physics* **2007**, *126*, 134116.

(42) Grimme, S. A simplified Tamm-Dancoff density functional approach for the electronic excitation spectra of very large molecules. *The Journal of Chemical Physics* **2013**, *138*, 244104.

(43) Niehaus, T. A.; Suhai, S.; Della Sala, F.; Lugli, P.; Elstner, M.; Seifert, G.; Frauenheim, T. Tight-binding approach to time-dependent density-functional response theory. *Phys. Rev. B* **2001**, *63*, 085108.

(44) Mokkath, J. H. Dopant-induced localized light absorption in CsPbX3 (X = Cl, Br, I) perovskite quantum dots. *New J. Chem.* **2019**, *43*, 18268–18276.

(45) Muhammed, M. M.; Mokkath, J. H. Linear acene molecules in plasmonic cavities: mapping evolution of optical absorption spectra and electric field intensity enhancements. *New J. Chem.* **2019**, *43*, 10774–10783.

(46) Casida, M. E.; Jamorski, C.; Casida, K. C.; Salahub, D. R. Molecular excitation energies to high-lying bound states from time-dependentdensity-functionalresponsetheory: Characterizationand correctionofthetime-dependentlocaldensityapproximation ionization threshold. *The Journal of Chemical Physics* **1998**, *108*, 4439–4449.

(47) Rossi, T. P.; Zugarramurdi, A.; Puska, M. J.; Nieminen, R. M. Quantized Evolution of the Plasmonic Response in a Stretched Nanorod. *Phys. Rev. Lett.* **2015**, *115*, 236804.

(48) Rossi, T. P.; Kuisma, M.; Puska, M. J.; Nieminen, R. M.; Erhart, P. Kohn–Sham Decomposition in Real-Time Time-Dependent Density-Functional Theory: An Efficient

Tool for Analyzing Plasmonic Excitations. *Journal of Chemical Theory and Computation* **2017**, *13*, 4779–4790, PMID: 28862851.